Smart Structures and Systems, *Vol. 35, No. 1 (2025) 15-28*
https://doi.org/10.12989/sss.2025.35.1.015

Novel offline iterative hybrid testing method based on model identification and correction

Tao Wang [1,3], Huan Zheng [1], Guoshan Xu*[2,3,4], Zhen Wang [5,6] and Liyan Meng [1]

[1] *School of Architecture and Engineering, Heilongjiang University of Science and Technology, Harbin 150022, China*
[2] *School of Civil Engineering, Harbin Institute of Technology, Harbin 150090, China*
[3] *Key Lab of Structures Dynamic Behavior and Control, Ministry of Education, Harbin Institute of Technology, Harbin 150090, China*
[4] *Key Lab of Intelligent Disaster Mitigation, Ministry of Industry and Information Technology, Harbin 150090, China*
[5] *School of Civil Engineering and Architecture, Wuhan University of Technology, Wuhan 430070, China*
[6] *Hainan Institute of Wuhan University of Technology, Sanya 572000, China*

(*Received February 2, 2024, Revised November 18, 2024, Accepted January 5, 2025*)

Abstract. The iterative hybrid testing (IHT) method, as one novel kinds of real-time hybrid testing (RTHT), provides a new technical support for disclosing the seismic performance of large-scale complex engineering structures. However, the IHT method adopts the methodology of direct whole time-history data exchange between the physical substructure (PS) and the numerical substructure (NS) based on the measured reaction forces of the PS, which results in the problems of slow iteration convergence speed and poor accuracy and stability. For solving these problems, one novel offline iterative hybrid testing method based on model identification and correction (IHT-MIC) is proposed in this paper. In the proposed IHT-MIC, the equivalent Maxwell model is used for precisely modelling the PS by parameter identification, and based on which the reaction force of the PS is corrected to improve the iteration convergence speed, accuracy, and stability. Firstly, the principle of the IHT-MIC is proposed. Furthermore, the numerical simulations and experimental tests are presented for validating the effectiveness and accuracy of the proposed method. It is shown from the numerical and experimental results that the least square method can accurately identify the parameters of Maxwell model, and the Maxwell model can effectively correct the reaction forces of the PS, which indicates that the accuracy of the IHT-MIC is greatly improved. Furthermore, compared with the traditional IHT, the IHT-MIC significantly improves the iteration convergence speed, reduces the oscillation amplitude during the iteration process. The proposed method may have broad application prospects in the fields of engineering structures with velocity-dependent energy dissipators.

Keywords: force correction; hybrid testing; maxwell model; model identification; offline iterative; viscous damper

1. Introduction

1.1 Background and motivation

Quasi-static testing (QST) (Clay and Knoth 2017), pseudo-dynamic testing (PDT) (Di Sarno *et al*. 2021), shaking table testing (STT) (Shing *et al*. 1996, Shen *et al*. 2020, Cao and Khan 2021) and real-time hybrid testing (RTHT) (Nakashima *et al*. 1992, Gomez *et al*. 2015, Ligeikis and Christenson 2020, Najafi *et al*. 2023, Xu *et al*. 2024) are the main test methods to obtain the seismic performance of engineering structures. Compared to others, the RTHT divides the overall structure into physical substructure (PS) and numerical substructure (NS) to obtain higher test accuracy with lower test cost. With the continuous improvement of RTHT technology, high-performance computer, and high-precision loading system, the RTHT was widely used in structural engineering (Li *et al*. 2022, Condori *et al*. 2023), non-structural element (Cao *et al*. 2024, Lu *et al*. 2019), bridge engineering (Lu *et al*. 2023, Park *et al*. 2023, Cai *et al*. 2009, Xao *et al*. 2012), marine engineering (Ransley *et al*. 2023, Vilsen *et al*. 2019), traffic engineering (Jiang *et al*. 2013, Koganei *et al*. 2017), vehicle engineering (Batterbee and Sims 2007, Muthalif *et al*. 2017), and other fields. At present, the main factors limiting the accuracy of RTHT are the computational efficiency and the stability of integration algorithms, the accuracy of the NS, the loading rate and accuracy of the PS, as well as the establishment of boundary conditions (Silva *et al*. 2020, Tsokanas *et al*. 2022). For solving these problems, many scholars have carried out a lot of researches in the fields of integration algorithms (Phillips *et al*. 2014, Li *et al*. 2020, Huang *et al*. 2022), time delay compensation (Horiuchi and Konno 2001, Chen *et al*. 2012, Strano and Terzo 2016), model parameter identification (Elanwar and Elnashai 2016, Yang *et al*. 2017), and so on. The research results further strengthen the development and application of RTHT. However, the RTHT will be confronted with great challenges, *e.g*., the high-precision simulation model of the NS can improve the accuracy of numerical calculation, whilst it will also produce higher computational delay and reduce the test accuracy. This problem is caused by the test characteristics

*Corresponding author, Ph.D., Professor,
E-mail: xuguoshan@hit.edu.cn

ISSN: 1738-1584 (Print), 1738-1991 (Online)

and is difficult to be completely addressed by the existing technology.

For solving the above problems, an iterative hybrid testing (IHT) method (Guo *et al*. 2016) was proposed. In this method, the numerical simulation and physical loading are divided into two relatively independent parts, which are independently carried out in the entire duration of the seismic action. Data exchange is not carried out in the manner of step-by-step integration, while only take the whole time-history data exchange after the integration and loading process. In this way, the application of high-precision numerical model of the NS is possible, and the excellent numerical integration method in numerical simulation can be used, and the effect of computational time delay is eliminated. In addition, since the physical loading is the specified path loading, the difficulty of compensating the physical time delay is greatly reduced.

There are two types of IHT. One is building a numerical model to replace the PS based on the reaction force response of the PS, *e.g*., the accurate discrete transfer function model (Guo and Pan 2024), the neural network model (Gao *et al*. 2023), the linear substitution model (Wang *et al*. 2022), and continuously optimizes the accuracy of the model through multiple numbers of iterative loading, so as to replace the physical model for pure numerical simulation of overall structure to solve the structural response. Another one is that the reaction force response of the PS is directly brought into the equation of motion to participate in the numerical calculation, and the convergence judgment is carried out through the outer loop control, *e.g*., the global iteration real-time hybrid testing (GI-RTHT) (Guo *et al*. 2018), the offline iterative hybrid simulation(OIHS) method combined with the fixed-point iteration(FPI) algorithm (Guo *et al*. 2022), the real-time hybrid simulation method based on multitasking loading (RHSM-ML) (Wang *et al*. 2023), the time-history iteration (THI) algorithm based on cumulative increments of OIHS (Guo *et al*. 2024). These methods do not require parameter identification, but because of the low frequency data exchange, the reaction force of the PS is not synchronized with the solved equation of motion. This misalignment results in decreased iteration convergence speed, compromised numerical stability, and limited practical application and development of the IHT.

1.2 Scope

From previous background introductions one can conclude that the traditional IHT method significantly reduces the frequency of data interaction between the NS and the PS. However, this leads to a lag in physical loading by one iteration round compared to pure numerical calculation. This lag introduces errors in the numerical model or equation of motion solution, whether by establishing a numerical model of PS using reaction time-history or directly incorporating it into the equation of motion for numerical calculation. Consequently, it reduces the convergence speed, numerical accuracy, and stability of the IHT. For solving these problems, a novel offline iterative hybrid testing method based on model identification and correction (IHT-MIC) is proposed in this paper. The main contents of this paper are as follows. The principle of the IHT-MIC method is proposed in Section 2. The proposed IHT-MIC is verified by numerical simulations of single-story and three-story frames in Section 3. The experimental tests of a three-story frame will be presented in Section 4. The conclusions are summarized in Section 5.

2. Principle of IHT-MIC

2.1 Methodology of IHT-MIC

The IHT adopts the concept of iteration in the RTHT. The equation of motion in IHT is shown in Eq. (1).

$$\mathbf{M}_{\mathrm{N}}\mathbf{a}_{\mathrm{N},i}^{j}+\mathbf{C}_{\mathrm{N}}\mathbf{v}_{\mathrm{N},i}^{j}+\mathbf{K}_{\mathrm{N}}\mathbf{d}_{\mathrm{N},i}^{j}+\mathbf{R}_{\mathrm{E},i}^{j}=\mathbf{F}_{i} \tag{1}$$

where **M**, **C**, and **K** are the mass, damping, and stiffness matrices, respectively; **a**, **v**, and **d** are the acceleration, velocity, and displacement vectors, respectively; $\mathbf{R}_{\mathrm{E}}$ and **F** are the reaction force vector of the PS and the external load vector, respectively; subscripts N and E denote the numerical substructure and the physical substructure, respectively, subscript i denotes the integration time step, $1 \le i \le n$; superscript j denotes the iteration round, $0 \le j \le j_{max}$.

The data exchange of the traditional IHT is shown in Fig. 1(a). It can be seen that after completing the whole time-history numerical calculation of j^{th} iteration round, the time-history loading commands $\mathbf{v}_{\mathrm{E}}^{j}$ and $\mathbf{d}_{\mathrm{E}}^{j}$ are transmitted to the loading system. The loading system carries out the time-history loading of the PS and measures the whole time-history reaction force $\mathbf{R}_{\mathrm{E}}^{j}$.

According to Eq. (1), in conducting the numerical calculation for the $(j+1)^{\mathrm{th}}$ iteration round, the reaction force

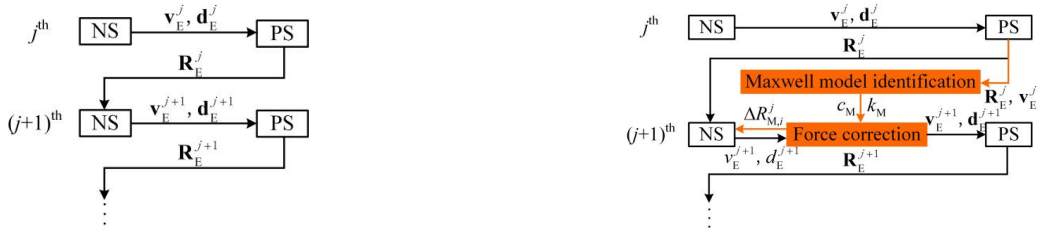

(a) IHT (b) IHT-MIC

Fig. 1 Data exchange diagram of IHT and IHT-MIC

of the $(j+1)^{\text{th}}$ iteration round $\mathbf{R}_{\text{E}}^{j+1}$ should be taken into consideration. However, as the value of $\mathbf{R}_{\text{E}}^{j+1}$ has not yet been measured, it is necessary to subsequently transmit the measured reaction force $\mathbf{R}_{\text{E}}^{j}$ to the NS for the numerical calculation of the $(j+1)^{\text{th}}$ iteration round, which inevitably leads to the issue of iteration round lag. The iteration round lag may lead to the error of solving the equation of motion, reduce iteration convergence speed, and decline the accuracy and stability of numerical calculation.

To solve this problem, this paper proposes an IHT-MIC method, a correction force is incorporated into the numerical computation by the IHT-MIC method. Specifically, the correction force represents the difference between the PS reaction force of the current iteration and the real PS reaction force of the previous iteration, which can be expressed as

$$\Delta\mathbf{R}_{\text{E}}^{j} = \mathbf{R}_{\text{E}}^{j} - \mathbf{R}_{\text{E}}^{j-1} \tag{2}$$

It can be seen that the correction force is a function of the PS reaction forces between adjacent iterative rounds, as the reaction forces of the PS in the previous iterative round $\mathbf{R}_{\text{E}}^{j-1}$ have been measured, but the reaction forces of the current iterative round $\mathbf{R}_{\text{E}}^{j}$ have not yet been loaded, so the correction force cannot be obtained directly. However, if a physically accurate numerical model of the substructure can be established, the correction force $\Delta\mathbf{R}_{\text{E}}^{j}$ can be calculated based on the model by calculating the substructure response between adjacent iterative rounds, and then incorporated into the equation of motion for numerical calculation to some extent, which can improve the numerical calculation accuracy and speed up and improve the convergence of the iteration.

The data interaction form of the IHT-MIC method is shown in Fig. 1(b), where c_{M} and k_{M} are the damping and stiffness of Maxwell model equivalent to PS, respectively. ΔR_{M} is the corrected force. Compared with the traditional IHT method, the IHT-MIC constructs an equivalent Maxwell model by collecting the force-velocity relationship of the PS after iterative numerical calculation and loading. At the same time of the step-by-step numerical calculation, the Maxwell model is used to gradually modify the reaction force through the historical and current responses of the PS, so as to reduce the error of solving the equation of motion, improve the iteration convergence speed, accuracy and stability of the numerical calculation.

The Maxwell model, as shown in Fig. 2, is a commonly used equivalent model of the viscous damper (Mathur and Khandelwal 2017), which simulates the viscous damper with a series of stiffness and damping elements. In Fig. 2, d_{C}, v_{C}, and a_{C} are the displacement, velocity, and acceleration of the damping element, respectively; d_{E}, v_{E}, and a_{E} are the total displacement, velocity, and acceleration of stiffness and damping elements, respectively; R_{M} is the reaction force of the PS.

The output reaction force of the Maxwell model is the displacement-dependent restoring force or the velocity-dependent damping force, *i.e.*

$$R_{\text{M}} = c_{\text{M}}v_{\text{C}} = k_{\text{M}}(d_{\text{E}} - d_{\text{C}}) \tag{3}$$

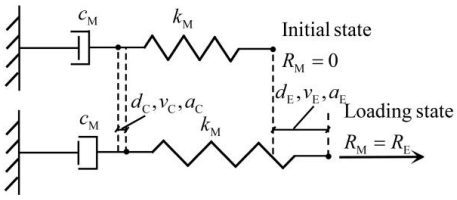

Fig. 2 Schematic diagram of Maxwell model

The most advantage of the Maxwell model is simplicity and adaptability. Furthermore, it can well reflect the relaxation phenomenon of viscoelastic dampers and the change trend of storage modulus with frequency, especially for viscous dampers with strong frequency dependence (Zhou *et al*. 2018). It can be seen from Eq. (3) that the reaction force of the Maxwell model is directly proportional to the velocity of the damping element or the displacement of the stiffness element. Therefore, the correction value for reaction force can be determined by analyzing the historical responses of the PS. The core of the IHT-MIC includes parameter identification of Maxwell model and reaction force correction of the PS.

2.2 Parameter identification

From Eq. (3), one can calculate the differential form of the reaction force about time is

$$\dot{R}_{\text{M}} = k_{\text{M}}(v_{\text{E}} - v_{\text{C}}) = k_{\text{M}}v_{\text{E}} - k_{\text{M}}v_{\text{C}} \tag{4}$$

From Eq. (3), one can also calculate

$$v_{\text{C}} = \frac{R_{\text{M}}}{c_{\text{M}}} \tag{5}$$

By substituting Eq. (5) into Eq. (4), one can obtain

$$\dot{R}_{\text{M}} = k_{\text{M}}v_{\text{E}} - \frac{k_{\text{M}}}{c_{\text{M}}}R_{\text{M}} \tag{6}$$

It can be seen from Eq. (6) that the derivative of Maxwell damper output is linearly related to the total velocity v_{E} and the damper output reaction force R_{M}, which indicates Eq. (6) is a first-order differential equation about the R_{M}. The output reaction force R_{M} can be calculated directly in case of the values of parameters c_{M} and k_{M} are determined.

Taking c_{M} and k_{M} as unknowns, Eq. (6) can be regarded as a nonlinear equation. The c_{M} and k_{M} can be determined by the nonlinear model parameter identification methods, *e.g.*, UKF (Mandela *et al*. 2012). Since the process of parameter identification using nonlinear model parameter identification method is rather complicated, in order to simplify the process of parameter identification, a variable substitution approach is employed to convert the nonlinear equation into a linear one for identification by linear methods. Eq. (6) is written as follows

$$\mathbf{A\theta} = \dot{\mathbf{R}}_{\text{M}} \tag{7}$$

in which

$$\boldsymbol{\theta} = \begin{bmatrix}\theta_1\\ \theta_2\end{bmatrix}_{2\times1} = \begin{bmatrix} k_{\mathrm{M}} \\ -\dfrac{k_{\mathrm{M}}}{c_{\mathrm{M}}}\end{bmatrix}_{2\times1} \tag{8}$$

$$\mathbf{A} = [v_{\mathrm{E}}, R_{\mathrm{M}}]_{n\times2} = \begin{bmatrix} v_{\mathrm{E},1} & R_{\mathrm{M},1} \\ v_{\mathrm{E},2} & R_{\mathrm{M},2} \\ \vdots & \vdots \\ v_{\mathrm{E},\,n} & R_{\mathrm{M},\,n}\end{bmatrix} \tag{9}$$

$$\dot{\mathbf{R}}_{\mathrm{M}} = \left[\dot{R}_{\mathrm{M}}\right]_{n\times1} = \begin{bmatrix} \dot{R}_{\mathrm{M},1} \\ \dot{R}_{\mathrm{M},2} \\ \vdots \\ \dot{R}_{\mathrm{M},\,n}\end{bmatrix} \tag{10}$$

Bring Eq. (8) into Eq. (6) yields

$$\theta_1 v_{\mathrm{E}} + \theta_2 R_{\mathrm{M}} = \dot{R}_{\mathrm{M}} \tag{11}$$

Rewriting the above equation into matrix form, *i.e.*

$$\begin{bmatrix} v_{\mathrm{E},1} & R_{\mathrm{M},1} \\ v_{\mathrm{E},2} & R_{\mathrm{M},2} \\ \vdots & \vdots \\ v_{\mathrm{E},\,n} & R_{\mathrm{M},\,n}\end{bmatrix} \cdot \begin{bmatrix}\theta_1\\ \theta_2\end{bmatrix} = \begin{bmatrix} \dot{R}_{\mathrm{M},1} \\ \dot{R}_{\mathrm{M},2} \\ \vdots \\ \dot{R}_{\mathrm{M},\,n}\end{bmatrix} \tag{12}$$

After defining the parameters, the original nonlinear equation is transformed into a linear equation with θ as the unknown quantity, and the parameters can be identified by the least square method, *i.e.*

$$\mathbf{A}^{\mathrm{T}}\mathbf{A}\widehat{\boldsymbol{\theta}} = \mathbf{A}^{\mathrm{T}}\dot{\mathbf{R}}_{\mathrm{M}} \tag{13}$$

where $\widehat{\boldsymbol{\theta}} = \begin{bmatrix}\hat{\theta}_1\\ \hat{\theta}_2\end{bmatrix}_{2\times1}$ is identification value.

Because $\mathbf{A}^{\mathrm{T}}\mathbf{A}$ is a reversible square matrix, the above formula can be transformed into

$$\widehat{\boldsymbol{\theta}} = (\mathbf{A}^{\mathrm{T}}\mathbf{A})^{-1}\mathbf{A}^{\mathrm{T}}\dot{\mathbf{R}}_{\mathrm{M}} \tag{14}$$

Eq. (14) can be used to determine the parameters $\widehat{\boldsymbol{\theta}}$ based on the structural response obtained by numerical calculation and physical loading during the hybrid testing.

2.3 Reaction force correction

With identified parameters $\widehat{\boldsymbol{\theta}}$, Eq. (11) can be expressed by

$$\hat{\theta}_1 v_{\mathrm{E},i} + \hat{\theta}_2 R_{\mathrm{M},i} = \dot{R}_{\mathrm{M},i} \tag{15}$$

The derivative of the reaction force of PS in Eq. (15) can be estimated by

$$\dot{R}_{\mathrm{M},i} = \frac{R_{\mathrm{M},i} - R_{\mathrm{M},i-1}}{\Delta t} \tag{16}$$

where Δt is the integration time step. By substituting Eq. (16) into Eq. (15), one can obtain

$$\hat{\theta}_1 v_{\mathrm{E},i} + \hat{\theta}_2 R_{\mathrm{M},i} = \frac{R_{\mathrm{M},i} - R_{\mathrm{M},i-1}}{\Delta t} \tag{17}$$

Based on Eq. (17), the reaction force of Maxwell model can be calculated as

$$R_{\mathrm{M},i} = \frac{\Delta t\hat{\theta}_1}{1-\Delta t\hat{\theta}_2} v_{\mathrm{E},i} + \frac{1}{1-\Delta t\hat{\theta}_2} R_{\mathrm{M},i-1} \tag{18}$$

The concept of iteration is introduced, and the reaction force of Maxwell model in jth iteration can be written as

$$R^{j}_{\mathrm{M},i} = \frac{\Delta t\hat{\theta}_1}{1-\Delta t\hat{\theta}_2} \cdot v^{j}_{\mathrm{E},i} + \frac{1}{1-\Delta t\hat{\theta}_2} R^{j}_{\mathrm{M},i-1} \tag{19}$$

Making a difference between the equations of motion of two adjacent iteration rounds, and use the historical response of the structure to calculate the correction force as

$$\begin{aligned}\Delta R^{j}_{\mathrm{M},i} &= R^{j}_{\mathrm{M},i} - R^{j-1}_{\mathrm{M},i} = \\ &\frac{\Delta t\hat{\theta}_1}{1-\Delta t\hat{\theta}_2}\left(v^{j}_{\mathrm{E},i} - v^{j-1}_{\mathrm{E},i}\right) + \frac{1}{1-\Delta t\hat{\theta}_2}\left(R^{j}_{\mathrm{M},i-1} - R^{j-1}_{\mathrm{M},i-1}\right)\end{aligned} \tag{20}$$

At the same time

$$\Delta R^{j}_{\mathrm{M},i-1} = R^{j}_{\mathrm{M},i-1} - R^{j-1}_{\mathrm{M},i-1} \tag{21}$$

Bring Eq. (21) into Eq. (20) and expand it to multi-degree of freedom structure, *i.e.*

$$\Delta\mathbf{R}^{j}_{\mathrm{M},i} = \frac{\Delta t\hat{\theta}_1}{1-\Delta t\hat{\theta}_2}\left(\mathbf{v}^{j}_{\mathrm{E},i} - \mathbf{v}^{j-1}_{\mathrm{E},i}\right) + \frac{1}{1-\Delta t\hat{\theta}_2}\Delta\mathbf{R}^{j}_{\mathrm{M},i-1} \tag{22}$$

Eq. (22) can be further simplified into a continuous differential form, *i.e.*

$$\Delta\dot{\mathbf{R}}^{j}_{\mathrm{M},i} = \hat{\theta}_1\left(\mathbf{v}^{j}_{\mathrm{E},i} - \mathbf{v}^{j-1}_{\mathrm{E},i}\right) + \hat{\theta}_2\Delta\mathbf{R}^{j}_{\mathrm{M},i} \tag{23}$$

Therefore, for the IHT-MIC proposed in this paper, the equation of motion solved by numerical calculation is shown in Eq. (24), *i.e.*

$$\mathbf{M}_{\mathrm{N}}\mathrm{a}^{j}_{\mathrm{N},i} + \mathbf{C}_{\mathrm{N}}\mathbf{v}^{j}_{\mathrm{N},i} + \mathbf{K}_{\mathrm{N}}\mathbf{d}^{j}_{\mathrm{N},i} + \mathbf{R}^{j-1}_{\mathrm{E},i} + \Delta\mathbf{R}^{j}_{\mathrm{M},i} = \mathbf{F}_i \tag{24}$$

It can be seen that for the IHT-MIC, the correction force is related to the difference between the relative velocities of two adjacent iteration rounds, where $\mathbf{v}^{j}_{\mathrm{E},i}$ can be solved by step-by-step integration of current iteration round or displacement difference; at the same time, it is related to the correction force of the previous step in the current iteration.

2.4 Implementation process

The implementation flow diagram of the proposed IHT-MIC is shown in Fig. 3, where the meanings of variables *i*, *j*, and *n* are referred to Eq. (1). The main implementation process is as follows.

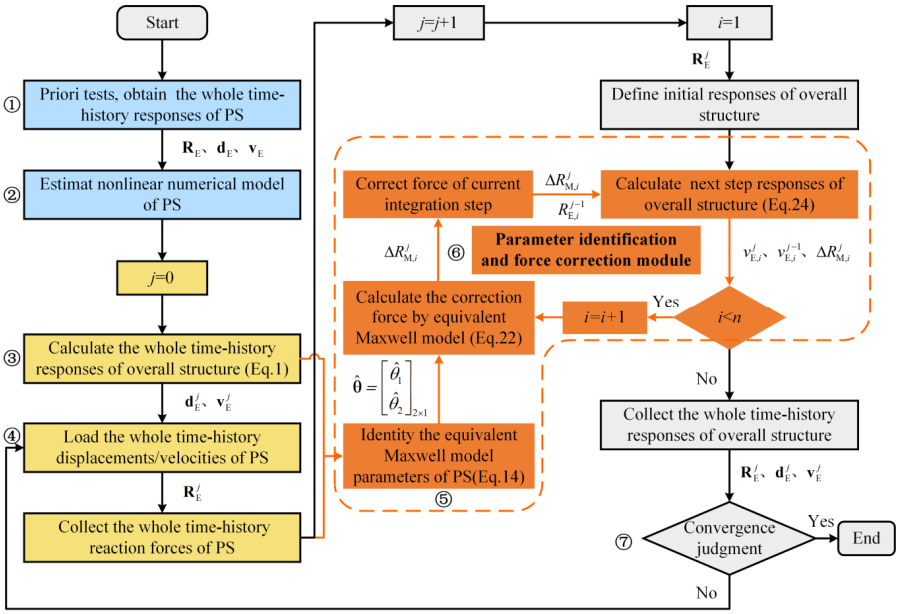

Fig. 3 Implementation flow diagram of IHT-MIC

① Prior tests. Initializes all parameters, including the NS, the step-by-step integration algorithm, *etc*., inputs seismic excitation and carries out whole time-history calculation, loads the PS and measures corresponding reaction force responses and the displacement responses of the PS.

② Preliminarily estimates the nonlinear model of the PS. Based on the measured force-displacement relationship, preliminarily establishes a nonlinear numerical model of the PS, which may have nonnegligible errors. Similar to the IHT method (Guo *et al*. 2016), the numerical model of the PS should conform to its actual hysteretic characteristics as closely as possible.

③ Calculates the whole time-history responses of overall structure. The pure numerical simulation of RTHT is carried out based on the nonlinear numerical model of the PS and the measured reaction forces.

④ Loads the PS with whole time-history displacement and velocity, and measures corresponding whole time-history reaction forces of the PS.

⑤ Identifies the equivalent Maxwell model parameter of the PS based on the latest force-velocity relationship of the PS at each iteration round.

⑥ Calculates the correction forces with the updated Maxwell model and conducts numerical calculation. Start the next round iteration calculation, take the reaction force of the previous iteration into the equation of motion, and correct the reaction force through Maxwell model of the PS to improve the accuracy of numerical calculation. Calculates the next step responses of overall structure.

⑦ Convergence judgment. Judges the convergence of the structural response according to the convergence evaluation indexes. If converges, completes the test; otherwise, returns to step ④.

Compared with RTHT and pure numerical simulation, the IHT-MIC method circumvents the issues of numerical calculation stability and time delay through iteration, and enhances the convergence speed and accuracy of the iteration. However, this method also imposes new requirements on the PS. Since the PS needs to undergo whole time-history loading in each iteration round, it implies that the PS should possess repeatable loading characteristics, such as dampers, elastic rubber bearings, etc. If the PS may encounter irrecoverable elastoplastic deformation or even failure during the test process, it is advisable to consider fabricating multiple specimens with minor differences using the same process to meet the requirements of iterative loading.

3. Numerical simulations

3.1 Single-story frame

To verify the effectiveness and applicability of the proposed method, numerical simulations on a single-story frame installed with Kelvin shock absorber were conducted by the traditional IHT and the proposed IHT-MIC. The structural framework diagram is shown in Fig. 4, where the NS is the main body of the framework, and the PS is the shock absorption device installed inside the framework expressed by one spring damping parallel Kelvin model.

The structural parameters are shown in Table 1. At the start iteration, set the numerical model accuracy to be 50% of the PS is shown in Eq. (25), and identify the equivalent Maxwell model of the PS based on the corresponding force-velocity relationship is shown in Eq. (26). The El Centro (NS, 1940) earthquake wave record, with a duration of 20 s and a peak ground acceleration of 150 gal, was utilized as the excitation. The central difference method (Wu *et al*. 2005), with an integration time step of 0.01 s, was employed as the integration algorithm.

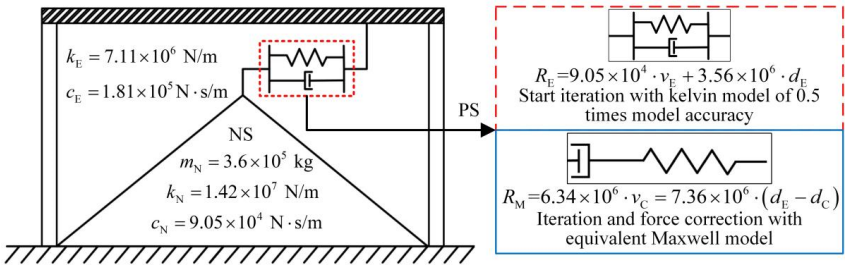

Fig. 4 Calculation diagram of single-story frame

Table 1 Structural parameters of single-story frame

Parameter	m (kg)	k (N/m)	c (Ns/m)
NS (single-story frame)	3.6×10^5	1.42×10^7	9.05×10^4
PS (Kelvin shock absorber)	0	7.11×10^6	1.81×10^5

The convergence step and root mean square error (RMSE) indexes are defined to analyze the following numerical and experimental results. The number of convergence step ε is shown in Eq. (27).

$$R_{\mathrm{E}} = 9.05 \times 10^4 \cdot v_{\mathrm{E}} + 3.56 \times 10^6 \cdot d_{\mathrm{E}} \tag{25}$$

$$R_{\mathrm{M}} = 6.34 \times 10^6 \cdot v_{\mathrm{C}} = 7.36 \times 10^6 \cdot (d_{\mathrm{E}} - d_{\mathrm{C}}) \tag{26}$$

$$\varepsilon_i^j = \left| d_{\mathrm{E},i}^j - \bar{d}_i \right| \le \varepsilon_0 \tag{27}$$

where ε, $\bar{d}$, and ε_0 are convergence step, reference displacement and convergence step limit displace1
ment, respectively. The physical meaning of Eq. (27) is that the number of steps whose displacement difference between the current iteration round and the reference solution is less than the limit value ε_0. This index can directly reflect the integration steps of iterative convergence of the current iteration, and can directly reflect the convergence speed and convergence trend. The convergence step limit displacement ε_0 can be defined as 0.1% or less of the displacement time-history amplitude. For numerical simulations, the displacement of the referenced solution can be calculated by the accurate numerical model. For physical tests, the referenced solutions are the structural responses when the displacements do not change with the increase of iteration rounds.

The RMSE is shown in Eq. (28), which judges the convergence of iteration by observing the deviation degree between the structural displacement response and thereferenced displacement time-history signals.

$$\mathrm{RMSE}^j = \sqrt{\frac{\sum_{i=1}^n \left(d_{\mathrm{E},i}^j - \bar{d}_i\right)^2}{\sum_{i=1}^n \left(\bar{d}_i\right)^2}} \tag{28}$$

Fig. 5 shows the time-histories of the lateral displacement of the frame in the first five round iterations. The Y-axis on the left is the displacement of the IHT-MIC method, whilst the Y-axis on the right is the displacement of the IHT method. From Fig. 5, one can see obvious difference between the displacement of the IHT-MIC method and the referenced solution at the 1st round iteration, while the difference decreases significantly with the increase of iteration round, *e.g.*, the displacement time-history converges completely at the 5th round iteration. However, for the IHT method, one can see dig difference between the displacement of the IHT method and the referenced solution at the 1st round iteration. Worse still, the displacement time-history shows divergence trend starting from the 2nd round iteration. The results indicate that compared with the IHT method, the IHT-MIC method has better numerical stability under this condition.

The comparison of the RMSE and the convergence step between the IHT-MIC and IHT for single-story frame are shown in Fig. 6, in which the limited displacement$\varepsilon_0 =$ 0.1 mm. In Fig. 6(a), the Y-axis on the left is the RMSE of the IHT-MIC method, and the Y-axis on the right is the RMSE of the IHT method. One can see from Fig. 6(a) that for the case of the IHT-MIC, the RMSE reached its maximum value of 0.24 at the 1st round iteration, and then decreased rapidly with the increase of the iteration rounds, especially, the RMSE decreased to 0 at the 5th round iteration. From Fig. 6(b), one can also see that the convergence steps reached 2000 at the 5th round iteration, indicating that the iteration is complete convergence. However, for the case of IHT, the RMSE of the displacement rapidly increase with the increase of iteration rounds, especially, significant numerical instability and divergence trend of displacement time-history can be observed at the 5th round iteration. From Fig. 6(b), one can also observe negligible variation of the convergence step.

The complete convergence steps and RMES of the IHT are shown in Fig. 7, where the Y-axis on the left is the convergence round and the Y-axis on the right is the RMSE. It can be seen from Fig. 7 that for the IHT method, the RMSE reached its maximum value at the 48th round iteration, gradually decreased after several periods of oscillation, and finally decreased to 0 at the 120th round iteration. From Fig. 7, one can also see that the convergence step shows a linear growth trend with the increase of iteration rounds, and complete converges at the 120th round iteration. The results reflect the convergence characteristics of the IHT, that is, the instability of numerical calculation will affect the convergence speed of iteration, but will not reverse the iteration convergence trend. The results indicate that compared with IHT method, the IHT-MIC method has better iteration convergence speed, numerical accuracy and stability, and engineering applicability.

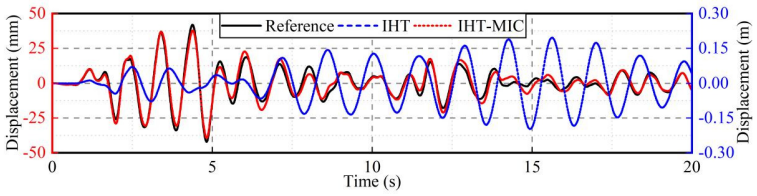

(a) 1st round iteration

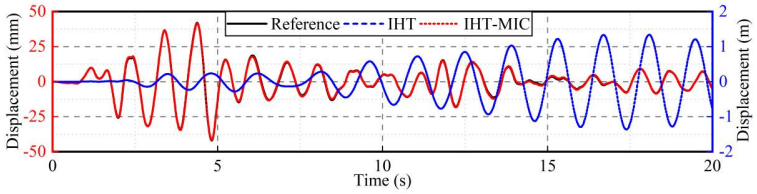

(b) 2nd round iteration

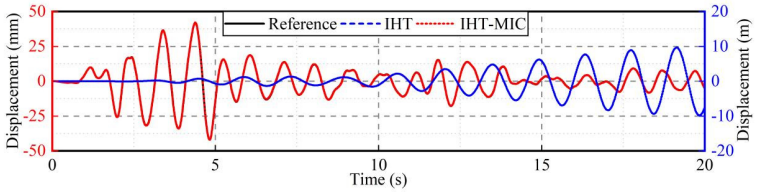

(c) 3rd round iteration

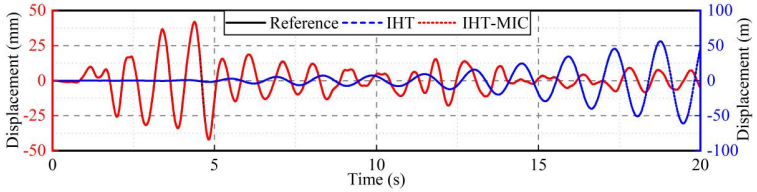

(d) 4th round iteration

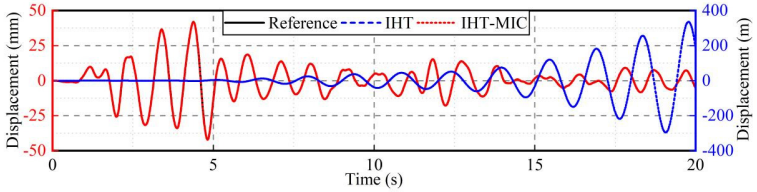

(e) 5th round iteration

Fig. 5 Simulation results of displacement time-history for single-story frame

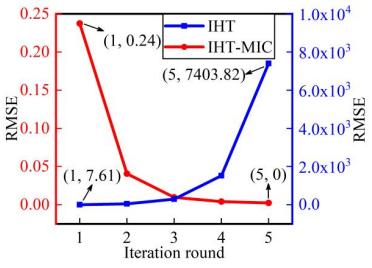

(a) RMSE

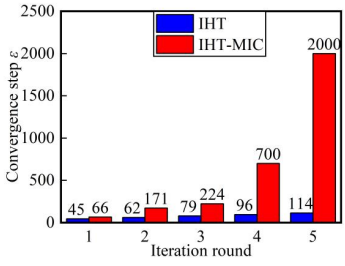

(b) ε

Fig. 6 RMSE and convergence steps of experimental results for single-story frame

In order to verify the applicability of the proposed method for multi-degree of freedom structures, numerical simulations were carried out for one three-story frame with viscous dampers. In this case, the NS was a three-story frame, and the PS was a viscous damper. The structural calculation diagram was shown in Fig. 8. The mass of each floor was set to be 2×10^4 kg, the interlayer stiffness was 4×10^7 N/m. The first three frequencies were 3.17, 8.88, and

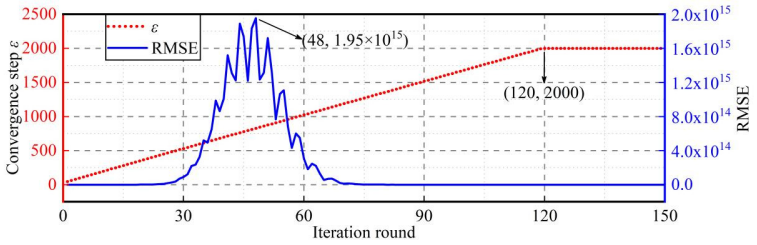

Fig. 7 RMSE and convergence steps indexes of IHT for single-story frame

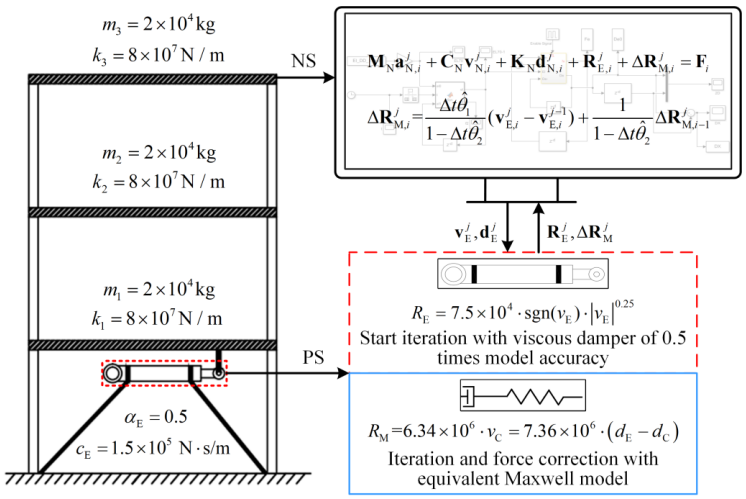

Fig. 8 Calculation diagram of numerical simulation of three-story frame

12.8 Hz, respectively. The structural damping matrix is shown in Eq. (29).

$$\mathbf{C} = \begin{bmatrix} 2.7004 & -1.0567 & 0 \\ -1.0567 & 2.7004 & -1.0567 \\ 0 & -1.0567 & 1.6437 \end{bmatrix} \times 10^4 \ \mathrm{Ns/m} \quad (29)$$

$$R_{\mathrm{E}} = 1.5 \times 10^5 \cdot sgn(v_{\mathrm{E}}) \cdot |v_{\mathrm{E}}|^{0.5} \quad (30)$$

$$R_{\mathrm{M}} = 6.34 \times 10^6 \cdot v_{\mathrm{C}} = 7.36 \times 10^6 \cdot (d_{\mathrm{E}} - d_{\mathrm{C}}) \quad (31)$$

The excitation was El Centro (NS, 1940) earthquake wave record with a duration of 10 s and a peak ground acceleration of 70 gal. The integration algorithm was the central difference method with an integration time step of 0.001 s. It should be noted that in order to avoid the influence of displacement divergence on the convergence speed, the positioning displacement limit of ±12 mm was set in the simulations.

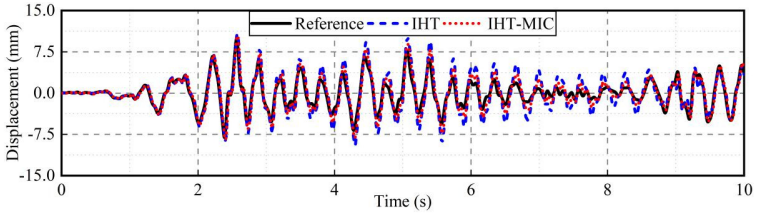

(a) 1st round iteration

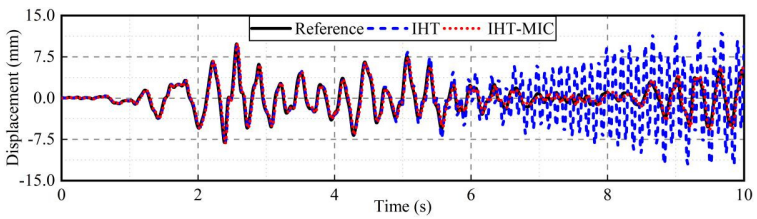

(b) 5th round iteration

Fig. 9 Simulation results of displacement time-histories for three-story frame

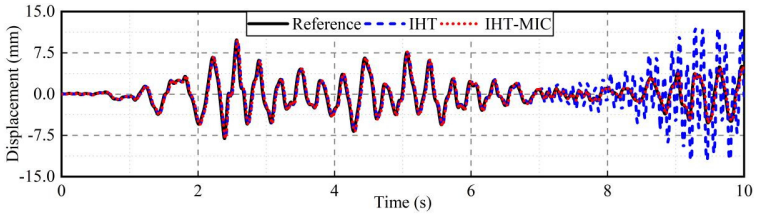

(c) 10th round iteration

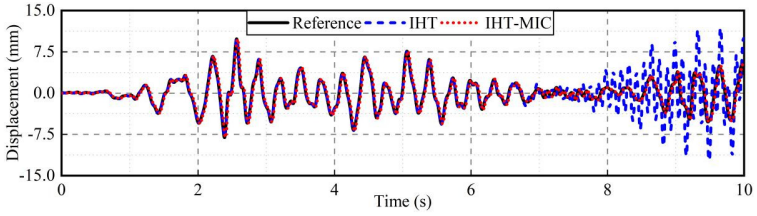

(d) 15th round iteration

Fig. 9 Continued

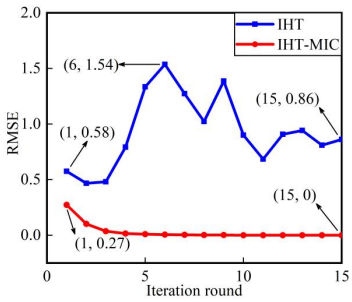

(a) RMSE

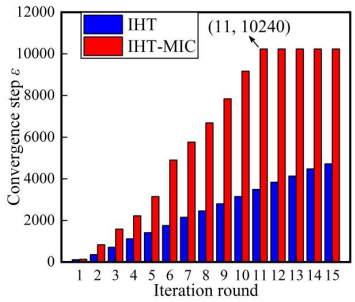

(b) ε

Fig. 10 RMSE and convergence steps of simulation results for three-story frame

3.2 Three-story frame with viscous damper

Fig. 9 is the time-histories comparison diagram of the lateral displacement on the first floor of the three-story frame during the 1st, 5th, 10th, and 15th iterations. It is shown from Fig. 9 that for the IHT-MIC, there was obvious error between the displacement time-history and the referenced solution at the 1st round iteration, and the error was gradually decreased to 0 with the increase of iteration rounds. While for the IHT, there was still an obvious error around the last 2s of the displacement time-history at the 15th iteration, and the displacement amplitude oscillates obviously even exceeds the limit several times.

Fig. 10 shows the RMSE and convergence step, respectively. Displacement limit of convergence step was $\varepsilon_0 = 0.1$ mm. It can be seen from Fig. 10 that the RMSE of the IHT-MIC was 0.27 at the 1st round iteration, and then continuously decreased, and the RMSE was 0 at the 11th iteration round. For the convergence step ε, the method converged completely at the 11th iteration round. While, the RMSE of the IHT always fluctuated at a high level, reached up to 0.58, 1.54, 0.86 at the 1st, 6th, and 15th round iterations. The convergence steps of 15 iteration rounds were 4718, which does not fully converge. The simulation results indicate that the IHT-MIC has faster convergence speed and more stable numerical calculation.

4. Experimental validations

4.1 Experimental setups

Experimental tests were conducted for further validating the effectiveness of the proposed IHT-MIC. A three-story frame with viscous dampers was taken as the research object, and the schematic diagram of experimental test is shown in Fig. 11. The tests were carried out at the key lab of structures dynamic behavior and control of Harbin Institute of Technology. The PS was a certain type of viscous damper, which was loaded by servo-hydraulic actuators. The experiments presented in this paper employ PID control based on displacement feedback, and the physical loading delay is approximately 15 ms. Since the experiments in this paper mainly focus on the verification of the effectiveness of the method, delay compensation was not implemented during the experiments. Relevant studies on delay compensation will be further carried out in the subsequent work.

4.2 Numerical models

The NS and excitation load of the three-story frame were set to be the same with the three-story frame in Section 3.2. The numerical model of the specimen was

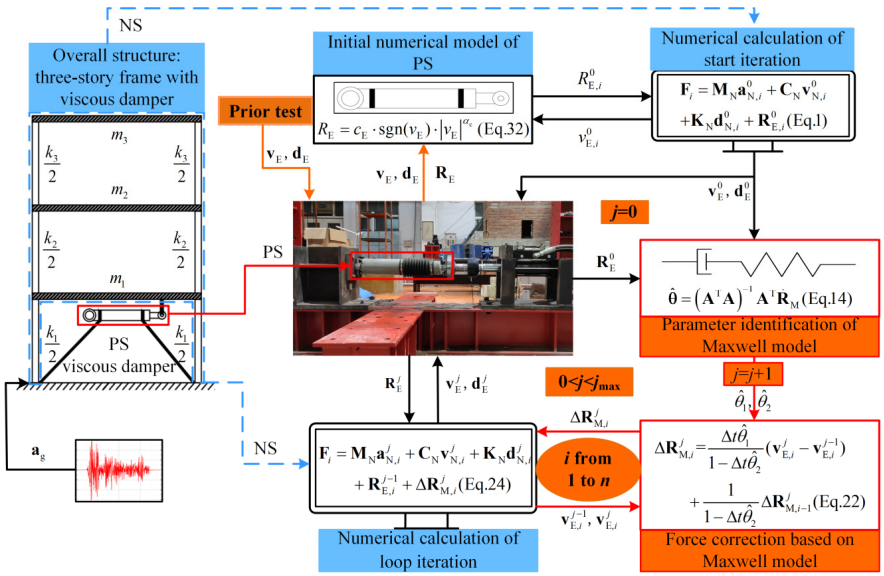

Fig. 11 Schematic diagram of experimental test for three-story frame

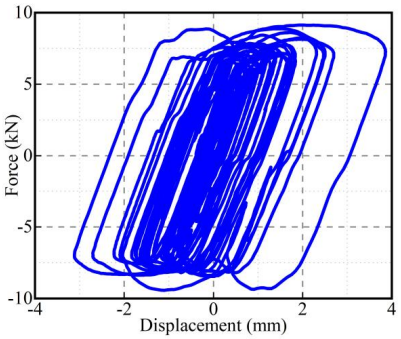

Fig. 12 Hysteretic curves of viscous damper

determined by the corresponding hysteretic curves of preliminary test, as shown in Fig. 12. According to the force-displacement relationship as shown in Fig. 12, the PS was equivalent to the exponential damper model. The numerical model of the PS of the start iteration was defined as

$$R_{\mathrm{E}} = 3.85 \times 10^4 \cdot sgn(v_{\mathrm{E}}) \cdot |v_{\mathrm{E}}|^{0.5} \tag{32}$$

At the same time, the equivalent Maxwell model parameters of the PS were identified according to the force-velocity relationship of the start iteration, *i.e.*

$$R_{\mathrm{M}}=1.98 \times 10^5 \cdot v_{\mathrm{C}} = 4.80 \times 10^6 \cdot (d_{\mathrm{E}} - d_{\mathrm{C}}) \tag{33}$$

To ensure the accuracy of parameter identification, it is necessary to verify the progress of the Maxwell model. The displacement and velocity time-histories were brought into the identified equivalent Maxwell model for calculating the reaction force. The corresponding calculated reaction force were compared with the referenced reaction force time-histories, as shown in Fig. 13. It can be seen from Fig. 13 that the identified result almost matches the referenced result, which indicates that the accuracy of the Maxwell model for parameter identification was high.

4.3 Results analysis

Fig. 14 shows the time-histories comparison diagram of the lateral displacement on the first floor of the three-story frame at the 1st, 5th, 10th, and 15th round iterations in the experimental tests. In order to avoid the influence of displacement divergence on convergence speed and damage to the loading system, the displacement limit of ±12 mm was set in the tests. At the 1st round iteration, both the IHT and the IHT-MIC had obvious errors. However, from the perspective of displacement amplitude, the IHT-MIC had obvious advantages over the IHT. In the subsequent iteration rounds, the IHT-MIC can converge at a faster speed, and the displacement amplitude was always in a relatively stable state. While for the IHT, the effective time steps were increasing, the growth speed was slow, and the displacement amplitude was oscillatory. The results indicate

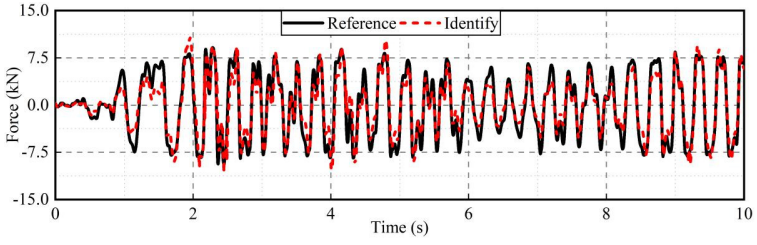

Fig. 13 Maxwell model verification

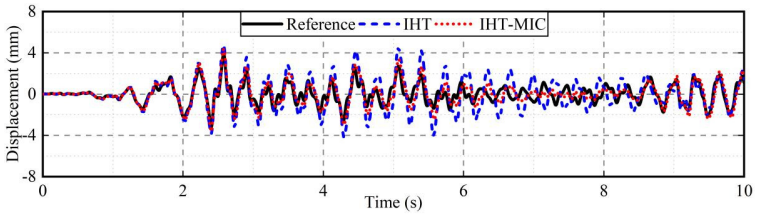

(a) 1st round iteration

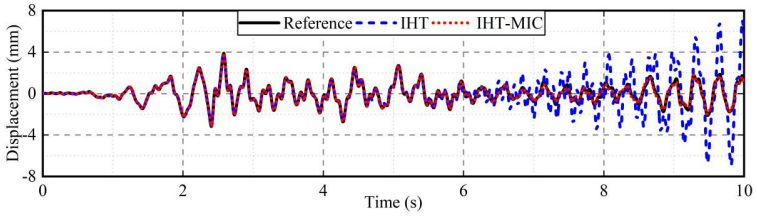

(b) 5th round iteration

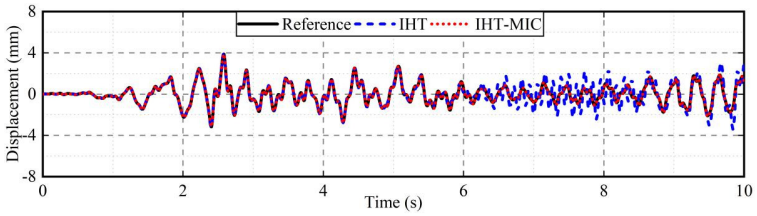

(c) 10th round iteration

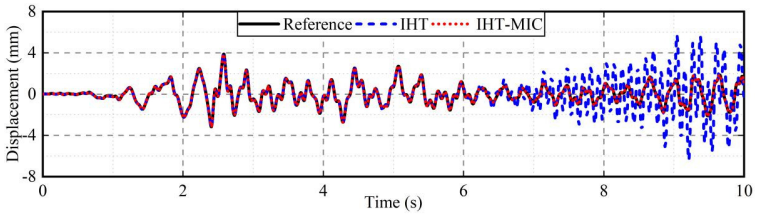

(d) 15th round iteration

Fig. 14 Experimental results of displacement time-histories for three-story frame

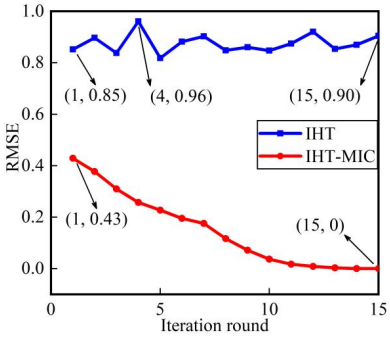

(a) RMSE

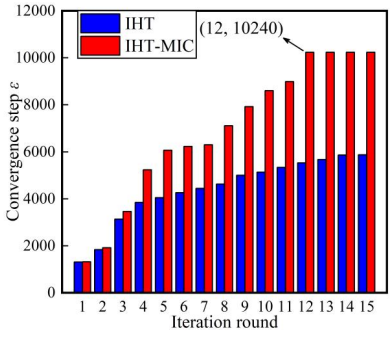

(b) ε

Fig. 15 RMSE and convergence steps of experimental results for three-story frame

that the IHT-MIC method has better convergence speed and numerical stability over the IHT.

Fig. 15 shows the RMES and the convergence steps of the experimental results of the displacement time-histories, respectively. Displacement limit of convergence step was $\varepsilon_0 = 0.1$ mm. For the IHT, the RMSE always fluctuated at a high level, *e.g.*, 0.85, 0.96, and 0.9 at the 1st, 4th, and 15th round iterations, and the iteration finally converged to 5878 steps at the 15th round iteration. While for the IHT-MIC, the RMSE decreased continuously after the start iteration, *e.g.*, the RMSE reaches the maximum value 0.43 at the 1st round iteration and decreased to 0 at the 15th round iteration. The IHT-MIC converged completely at the 12th round iteration, which indicates the IHT-MIC had better convergence speed

compared to the IHT. The experimental results can obtain similar conclusions with the simulation result as shown in Section 3.2.

5. Conclusions

For improving the convergence speed, accuracy, and stability of the iterative hybrid testing (IHT), a novel offline iterative hybrid testing method based on model identification and correction (IHT-MIC) was proposed in this paper. Numerical simulations and experimental tests indicate that this method has distinct superiority compared with the IHT method. The main conclusions are as follows.

- A novel IHT-MIC method was proposed. In this method, the equivalent Maxwell model of the PS is identified using the least squares method, and the reaction forces at the current step of the PS are corrected using the velocities from adjacent iteration rounds and the corrected forces from the previous integration step. By employing offline iteration and force correction, the IHT-MIC can effectively enhance the iterative convergence speed and reduce the number of iterations required for complete convergence.
- Numerical simulations were conducted for validating the effectiveness of the proposed methods. Numerical simulation results of the single-degree of freedom system show that the iteration round required for complete convergence of structural responses time-history is reduced from 120 of the IHT to 5 of the IHT-MIC, and the RMSE is reduced from divergence of the IHT to 0.24 of the IHT-MIC. Numerical simulation results of the three-story frame system also show that for the IHT-MIC, the RMSE reaches the maximum of 0.27 at the 1st round iteration and then decreases rapidly, and the IHT-MIC converged completely at the 11th round iteration. While for the IHT, the RMSE at the 15th round iteration is remain higher up to 1.54, and the IHT not completely converged. The numerical results indicate that compared with the IHT method, the IHT-MIC behaves faster convergence speed, higher numerical accuracy and stability.
- Experimental tests were conducted for validating the effectiveness of the proposed methods. Experimental results of the three-story frame system show that for the IHT-MIC, the RMSE reaches the maximum value of 0.43 at the 1st round iteration and decreases rapidly, and the IHT-MIC completely converged at 12th round iteration. While for the IHT, the RMSE always remain at a higher level, and the IHT not completely converged. The experimental results indicate that compared with the IHT, the IHT-MIC behaves faster convergence speed, higher numerical accuracy and stability.

The prospective works of this study are to investigate better parameter identification method of Maxwell model and to seek a more accurate nonlinear model of the PS to improve the efficiency and accuracy of the IHT-MIC.

Acknowledgments

The research described in this paper was financially supported by the National Natural Science Foundation of China (Grant Nos. 52278173, 52378150, 52078398) and the Foundation of Key Laboratory of Structures Dynamic Behavior and Control (Ministry of Education) in Harbin Institute of Technology (HITCE202008).

References

Batterbee, D.C. and Sims, N.D. (2007), "Hardware-in-the-loop simulation of magnetorheological dampers for vehicle suspension systems", *J. Syst. Control Eng.*, **221**(2), 265-278. https://doi.org/10.1243/09596518JSCE304

Cai, X., Tian, S., Wang, D. and Xao, Y. (2009), "Networked collaborative pseudo-dynamic testing of a multi-span bridge based on NetSLab", *Earthq. Eng. Eng. Vib.*, **8**, 387-397. https://doi.org/10.1007/s11803-009-8110-z

Cao, M. and Khan, M. (2021), "Effectiveness of multiscale hybrid fiber reinforced cementitious composites under single degree of freedom hydraulic shaking table", *Struct. Concrete*, **22**(1), 535-549. https://doi.org/10.1002/suco.201900228

Cao, Y., Qu, Z., Fu, H., Ji, X. and Chakraborty, S. (2024), "A substructural shake table testing method for full-scale nonstructural elements", *Mech. Syst. Signal. Process.*, **218**, 111575. https://doi.org/10.1016/j.ymssp.2024.111575

Chen, C., Ricles, J.M. and Guo, T. (2012), "Improved adaptive inverse compensation technique for real-time hybrid simulation", *J. Eng. Mech.*, **138**(12), 1432-1446. https://doi.org/10.1061/(ASCE)EM.1943-7889.0000450

Clay, S.B. and Knoth, P.M. (2017), "Experimental results of quasi-static testing for calibration and validation of composite progressive damage analysis methods", *J. Compos. Mater.*, **51**(10), 1333-1353. https://doi.org/10.1177/0021998316658539

Condori Uribe, J.W., Salmeron, M., Patino, E., Montoya, H., Dyke, S.J., Silva, C.E., Maghareh, A., Najarian, M. and Montoya, A. (2023), "Experimental benchmark control problem for multi-axial real-time hybrid simulation", *Front. Built Environ.*, **9**, 1270996. https://doi.org/10.3389/fbuil.2023.1270996

Di Sarno, L., Freddi, F., D'Aniello, M., Kwon, O.S., Wu, J.R., Gutiérrez-Urzúa, F., Landolfo, R., Park, J., Palios, X. and Strepelias, E. (2021), "Assessment of existing steel frames: Numerical study, pseudo-dynamic testing and influence of masonry infills", *J. Constr. Steel Res.*, **185**, 106873. https://doi.org/10.1016/j.jcsr.2021.106873

Elanwar, H.H. and Elnashai, A.S. (2016), "Framework for online model updating in earthquake hybrid simulations", *J. Earthq. Eng.*, **20**(1), 80-100. https://doi.org/10.1080/13632469.2015.1051637

Gao, F., Tang, Z. and Du, X. (2023), "Implementation of offline iterative hybrid simulation based on neural networks", *Earthq. Eng. Resili.*, **2**, 383-402. https://doi.org/10.1002/eer2.60

Gomez, D., Dyke, S.J. and Maghareh, A. (2015), "Enabling role of hybrid simulation across NEES in advancing earthquake engineering", *Smart Struct. Syst., Int. J.*, **15**(3), 913-929. https://doi.org/10.12989/sss.2015.15.3.913

Guo, Y.M. and Pan, P. (2024), "Accelerated time history iteration method for offline real-time hybrid testing", *Earthq. Eng. Struct. Dyn.*, **53**(9), 2805-2826. https://doi.org/10.1002/eqe.4133

Guo, J., Zhao, W., Du, Y., Chen, W. and Xu, R. (2016), "Real-time substructure test method applying global iteration and its verification", *J. Harbin. Eng. Univ.*, **37**(11), 1498-1503. [In Chinese] https://doi.org/10.11990/jheu.201606009

Guo, J., Zhao, W., Du, Y., Cao, Y., Wang, G. and Zhang, M. (2018), "New method for real-time hybrid testing with a global iteration strategy", *J. Struct. Eng.*, **144**(12), 04018218. https://doi.org/10.1061/(ASCE)ST.1943-541X.0002207

Guo, W., Long, Y., He, C., Wang, Y., Zeng, Y. and Song, J. (2022), "Off-Line Hybrid Simulation Method on Train-Track-Bridge Coupling Vibration in High-Speed Railway", *Int. J. Struct. Stab. Dyn.*, **22**(10), 2241014. https://doi.org/10.1142/S0219455422410140

Guo, Y., Wang, H. and Pan, P. (2024), "Time history iteration algorithm for offline real-time hybrid testing", *Earthq. Eng. Struct. Dyn.*, **53**(1), 432-450. https://doi.org/10.1002/eqe.4027

Horiuchi, T. and Konno, T. (2001), "A new method for compensating actuator delay in real-time hybrid experiments", *Phil. Trans. R. Soc. A*, **359**(1786), 1893-1909. https://doi.org/10.1098/rsta.2001.0878

Huang, L., Chen, C., Huang, S. and Wang, J. (2022), "Stability of real-time hybrid simulation involving time-varying delay and direct integration algorithms", *J. Vib. Control*, **28**(13-14), 1818-1834. https://doi.org/10.1177/10775463211001618

Jiang, Z., Kim, S.J., Plude, S. and Christenson, R. (2013), "Real-time hybrid simulation of a complex bridge model with MR dampers using the convolution integral method", *Smart Mater. Struct.*, **22**(10), 105008. https://doi.org/10.1088/0964-1726/22/10/105008

Koganei, R., Watanabe, N., Sasaki, K., Maki, Y., Yamaguchi, T. and Shimomura, T. (2017), "Development of virtual running test environment for railway vehicles based on Hardware-In-the-Loop Simulation to reproduce actual running on a track", *Mech. Eng. J.*, **4**(1), 1-12. https://doi.org/10.1299/mej.16-00516

Li, L., Wang, G., Zhang, X. and Yu, H. (2020), "Adaptive real-time recursive radial distance-time plane Hough transform track-before-detect algorithm for hypersonic target", *IET Radar, Sonar Navig.*, **14**(1), 138-146. https://doi.org/10.1049/iet-rsn.2019.0198

Li, H.W., Wang, F., Ni, Y.Q., Wang, Y.W. and Xu, Z.D. (2022), "An adaptive and robust control strategy for real-time hybrid simulation", *Sensors*, **22**(17), 6569. https://doi.org/10.3390/s22176569

Ligeikis, C. and Christenson, R. (2020), "Assessing structural reliability using real-time hybrid sub-structuring", *Int. J. Lifecycle Perform. Eng.*, **4**(1-3), 158-183. https://doi.org/10.1504/IJLCPE.2020.108934

Lu, L., Fermandois, G.A., Lu, X., Spencer, B.F. Jr., Duan, Y.F. and Zhou, Y. (2019), "Experimental evaluation of an inertial mass damper and its analytical model for cable vibration mitigation", *Smart Struct. Syst., Int. J.*, **23**(6), 589-613. https://doi.org/10.12989/sss.2019.23.6.589

Lu, L.Y., Lin, G.L., Lei, K.T., Yeh, S.W. and Liu, K.Y. (2023), "Accuracy assessment of real-time hybrid testing for seismic control of an offshore wind turbine supporting structure with a TMD", *Smart Struct. Syst., Int. J.*, **31**(6), 601-619. https://doi.org/10.12989/sss.2023.31.6.601

Mandela, R.K., Kuppuraj, V., Rengaswamy, R. and Narasimhan, S. (2012), "Constrained unscented recursive estimator for nonlinear dynamic systems", *J. Process Contr.*, **22**(4), 718-728. https://doi.org/10.1016/j.jprocont.2012.02.001

Mathur, V. and Khandelwal, K. (2017), "Flow of fractional maxwell fluid in oscillating pipe-like domains", *Int. J. Appl. Comput. Math.*, **3**, 841-858. https://doi.org/10.1007/s40819-016-0139-x

Muthalif, A.G., Kasemi, H.B., Nordin, N.D., Rashid, M.M. and Razali, M.K.M. (2017), "Semi-active vibration control using experimental model of magnetorheological damper with adaptive F-PID controller", *Smart Struct. Syst., Int. J.*, **20**(1), 85-97. https://doi.org/10.12989/sss.2017.20.1.085

Najafi, A., Fermandois, G.A., Dyke, S.J. and Spencer Jr, B.F. (2023), "Hybrid simulation with multiple actuators: A state-of-the-art review", *Eng. Struct.*, **276**, 115284. https://doi.org/10.1016/j.engstruct.2022.115284

Nakashima, M., Kato, H. and Takaoka, E. (1992), "Development of real-time pseudo dynamic testing", *Earthq. Eng. Struct. Dyn.*, **21**(1), 79-92. https://doi.org/10.1002/eqe.4290210106

Park, J., Park, M., Chae, Y. and Kim, C.Y. (2023), "Real-time hybrid simulation for investigating the influence of vertical ground motions on the lateral response of RC piers", *Earthq. Eng. Struct. Dyn.*, **52**(10), 2928-2944. https://doi.org/10.1002/eqe.3902

Phillips, B.M., Takada, S., Spencer Jr, B.F. and Fujino, Y. (2014), "Feedforward actuator controller development using the backward-difference method for real-time hybrid", *Smart Struct. Syst., Int. J.*, **14**(6), 1081-1103. https://doi.org/10.12989/sss.2014.14.6.1081

Ransley, E.J., Brown, S.A., Edwards, E.C., Tosdevin, T., Monk, K., Reynolds, A.M., Greaves, D. and Hann, M.R. (2023), "Real-Time Hybrid Testing of a Floating Offshore Wind Turbine Using a Surrogate-Based Aerodynamic Emulator", *ASME Open J. Eng. ASME*, **2**, 021017. https://doi.org/10.1115/1.4056963

Shen, Y.S., Wang, Z.Z., Yu, J., Zhang, X. and Gao, B. (2020), "Shaking table test on flexible joints of mountain tunnels passing through normal fault", *Tunn. Undergr. Sp. Tech.*, **98**, 103299. https://doi.org/10.1016/j.tust.2020.103299

Shing, P.B., Nakashima, M. and Bursi, O.S. (1996), "Application of pseudodynamic test method to structural research", *Earthq. Spectra*, **12**(1), 29-56. https://doi.org/10.1193/1.1585867

Silva, C.E., Gomez, D., Maghareh, A., Dyke, S.J. and Spencer Jr, B.F. (2020), "Benchmark control problem for real-time hybrid simulation", *Mech. Syst. Signal Pr.*, **135**, 106381. https://doi.org/10.1016/j.ymssp.2019. 106381

Strano, S. and Terzo, M. (2016), "Actuator dynamics compensation for real-time hybrid simulation: an adaptive approach by means of a nonlinear estimator", *Nonlinear Dyn.*, **85**(4), 2353-2368. https://doi.org/10.1007/s11071-016-2831-0

Tsokanas, N., Pastorino, R. and Stojadinović, B. (2022), "Adaptive model predictive control for actuation dynamics compensation in real-time hybrid simulation", *Mech. Mach. Theory*, **172**, 104817. https://doi.org/10.1016/j.mechmachtheory.2022.104817

Vilsen, S.A., Sauder, T., Sørensen, A.J. and Føre, M. (2019), "Method for real-time hybrid model testing of ocean structures: Case study on horizontal mooring systems", *Ocean Eng.*, **172**, 46-58. https://doi.org/10.1016/j.oceaneng.2018.10.042

Wang, Z., Lu, W., Wu, B. and Jia, X. (2022), "Iterative learning control method for shaking table test based on a surrogate specimen model", *China Civil Eng. J.*, **55**(S1), 203-208+256. [In Chinese] https://doi.org/10.15951/j.tmgcxb.2022.s1.0912

Wang, T., Hao, J., Xu, G., Wang, Z., Meng, L. and Zheng, H. (2023), "A real-time hybrid simulation method based on multitasking loading", *Struct. Des. Tall Spec.*, **32**(14-15), e2045. https://doi.org/10.1002/tal.2045

Wu, B., Bao, H., Ou, J. and Tian, S. (2005), "Stability and accuracy analysis of the central difference method for real-time substructure testing", *Earthq. Eng. Struct. Dyn.*, **34**(7), 705-718. https://doi.org/10.1002/eqe.451

Xao, Y., Guo, Y.R., Zhu, P.S., Kunnath, S. and Martin, G.R. (2012), "Networked pseudodynamic testing of bridge pier and precast pile foundation", *Eng. Struct.*, **38**, 32-41. https://doi.org/10.1016/j.engstruct.2011.12.020

Xu, G., Jiang, Y., Ning, X. and Liu, Z. (2024), "A real-time hybrid testing method for vehicle-bridge coupling systems", *Smart Struct. Syst., Int. J.*, **33**(1), 1-16. https://doi.org/10.12989/sss.2024.33.1.001

Yang, G., Wu, B., Ou, G., Wang, Z. and Dyke, S. (2017), "HyTest: platform for structural hybrid simulations with finite element model updating", *Adv. Eng. Softw.*, **112**, 200-210.

https://doi.org/10.1016/j.advengsoft.2017.05.007
Zhou, Y., Shi, F., Ozbulut, O.E., Xu, H. and Zi, D. (2018), "Experimental characterization and analytical modeling of a large-capacity high-damping rubber damper", *Sturct. Control Health Monitor*., **25**(6), e2183. https://doi.org/10.1002/stc.2183